*J. Fluid Mech.* (2000), *vol.* 424, *pp.* 1–20. Printed in the United Kingdom



# The effect of air swirl profile on the instability of a viscous liquid jet

By Y. LIAO[1], S. M. JENG[1], M. A. JOG[2] AND M. A. BENJAMIN[3]

[1]Department of Aerospace Engineering and Engineering Mechanics, University of Cincinnati, Cincinnati, OH 45221, USA

[2]Department of Mechanical, Industrial, and Nuclear Engineering, University of Cincinnati, Cincinnati, OH 45221, USA

[3]Parker Hannifin Corporation, Mentor, OH 44060, USA

(Received 3 December 1999 and in revised form 7 June 2000)

A temporal linear stability analysis has been carried out to predict the instability of a viscous liquid jet surrounded by a swirling air stream with three-dimensional disturbances. The effects of flow conditions and fluid properties on the instability of the liquid jet are investigated via a parametric study by varying axial Weber number axial velocity ratio of the gas to liquid phase, swirl Weber numbers, density ratio and the Ohnesorge number. It is observed that the relative axial velocity between the liquid and gas phases promotes the interfacial instability. As the axial Weber number increases, the growth rates of unstable waves, the most unstable wavenumber and the unstable range of wavenumbers increase. Meanwhile, the increasing importance of helical modes compared to the axisymmetric mode switches the breakup regime from the Rayleigh regime to the first wind-induced regime and on to the second wind-induced regime. The predicted range of wavenumbers in which the first helical mode has higher growth rates than the axisymmetric mode agrees very well with experimental data. Results show that the destabilizing effects of the density ratio and the axial Weber number are nearly the same. Liquid viscosity inhibits the disintegration process of the liquid jet by reducing the growth rate of disturbances and by shifting the most unstable wavenumber to a lower value. Moreover, it damps higher helical modes more significantly than the axisymmetric mode. Air swirl has a stabilizing effect on the liquid jet. As air swirl strength increases, the growth rates of helical modes are reduced more significantly than that of the axisymmetric mode. The air swirl profile is found to have a significant effect on the instability of the liquid jet. The global, as well as local, effects of the swirl profile are examined in detail.

## 1. Introduction

Atomization of liquid jets is fundamental to many industrial applications such as fuel injectors in internal combustion engines, liquid fuel rocket engines, afterburners of gas turbine engines, spray coating of surface materials, and agriculture sprays. The breakup process of the liquid jet is affected by a large number of factors, including flow conditions, fluid properties and nozzle geometry (Lin & Reitz 1998). The various forces involved in the breakup process are inertial, surface tension, aerodynamic, centrifugal, and viscous. Some of the forces resist the disintegration process while others promote it. It is the competition among these forces that determines the instability of the liquid

jet. Understanding the specific role of each force in the breakup process will benefit not only fuel injector design but also the numerical simulation of spray combustion.

Following Rayleigh's pioneering work (Rayleigh 1892), extensive studies have been conducted on temporal as well as spatial instability from low to high jet velocity (Lin & Reitz 1998). Four different breakup regimes have been identified that correspond to different manifestations of the jet as the flow conditions are changed (Reitz & Bracco 1982, 1986; Lefebvre 1989; Lin & Reitz 1998). These regimes are called the Rayleigh regime, the first wind-induced regime, the second wind-induced regime, and the atomization regime. In the Rayleigh regime, that is at very low jet velocity, surface tension is the driving force for the growth of unstable waves formed at the interface and the jet is broken up by the axisymmetric mode. The instability of a liquid jet in the Rayleigh regime is summarized by Sterling & Sleicher (1975). In the first wind-induced regime, the aerodynamic interaction between the liquid and the ambient gas becomes important and the appearance of the jet becomes sinuous (asymmetric) before breakup occurs. The size of drops formed in both the Rayleigh regime and the first wind-induced regime is of the order of the jet diameter. In the second wind-induced regime, drops are produced by shear waves on the jet surface and breakup occurs several diameters downstream of the nozzle exit. In the atomization regime, however, drops of sizes much smaller than the jet diameter are formed on the jet surface and the jet breaks up immediately at the nozzle exit. Large discrepancies exist between theoretical predictions of the intact length and spray angle, and measured data. Various mechanisms have been proposed to explain the differences. These include aerodynamic interaction theory, liquid turbulence, cavitation inside the nozzle, velocity profile relaxation, and liquid supply pressure oscillation (Reitz & Bracco 1982). After evaluation of these mechanisms based on their extensive experiments, Reitz & Bracco (1982) found that no single mechanism could fully explain the jet atomization process. However, they concluded that the combination of aerodynamic interaction theory and nozzle geometry was effective in explaining their experimental results. Recent studies (Mansour & Chigier 1994; Faeth, Hsiang & Wu 1995) have shown that turbulence generated in the flow passage has a significant effect on jet breakup properties. Also, papers by Lin & Ibrahim (1995) and Lin & Chen (1998) demonstrated that interfacial shear and pressure fluctuation work together to cause the Taylor-mode instability, which leads to droplets of diameter much smaller than the jet diameter. It is now generally agreed that, among various mechanisms, the aerodynamic interaction between the liquid and the ambient gas plays an important role in the breakup of the liquid jet (Reitz & Bracco 1982; Lin & Reitz 1998). It is also well established that the drop sizes are related to the most unstable wavelength and the intact length depends on the maximum growth rate. Therefore, linear stability analysis based on aerodynamic interaction theory can provide important guidance in determining the breakup behaviour of the liquid jet.

In the existing aerodynamic interaction theory (Levich 1962; Sterling & Sleicher 1975; Reitz & Bracco 1982; Lin & Kang 1987), disturbances were assumed to be axisymmetric. However, a number of experimental studies (Hoyt & Taylor 1977; Chigier 1989; Krulle, Mayer & Schley 1990) have revealed the presence of three-dimensional disturbances on the jet surface at high jet velocity. Yang (1992) was the first to theoretically consider the asymmetric instability of an inviscid liquid jet and found that sinuous modes become dominant in a certain wavelength range at high jet velocity. Lin & Webb (1994) and Li (1995) extended Yang's work by including liquid viscosity. However, the question regarding which mode – the axisymmetric mode or a helical mode – the liquid viscosity damps more significantly still remains unclear.

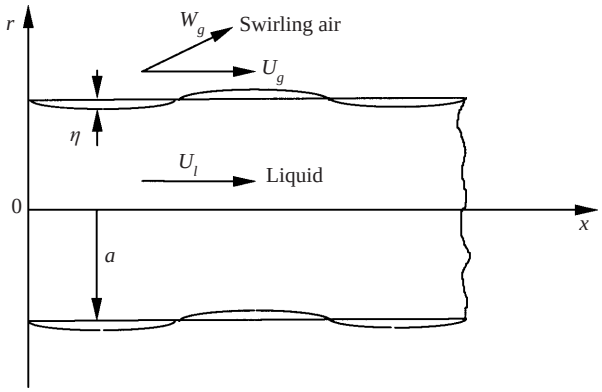


FIGURE 1. A liquid jet surrounded by swirling air.

More importantly, the flow conditions considered in these studies are quite different from those involved in practical fuel injection processes of combustion engines, and air swirl and swirl profile effects have not be examined.

The objective of the present paper is to develop an advanced theoretical model to predict the instability of a viscous liquid jet subjected to a swirling air stream and three-dimensional disturbances. In the model, the ambient air is assumed to move with axial as well as tangential velocity components. This flow condition is expected to reveal essential physics underlying the practical fuel atomization process (Heywood 1988; Weaving 1990). Efforts have been made to understand how flow conditions and fluid properties affect the growth rates of various helical modes in addition to that of the axisymmetric mode under no-swirl and swirling flow conditions. To investigate the effect of air swirl profile, the tangential velocity profile is chosen to be a combination of free-vortex and solid-body-rotation types as a general swirl profile can be constructed from them. The global and local effects of air swirl profile on the instability of the liquid jet are formulated and examined in detail.

## 2. Mathematical formulation

The stability model considers a moving viscous liquid jet surrounded by a coaxial swirling air stream as shown in figure 1. Both the liquid and the gas are assumed to be incompressible and gravity force is neglected. The ambient air is considered inviscid because inclusion of gas viscosity makes it extremely difficult to obtain the solution for the swirling air stream which exactly satisfies the Navier–Stokes equations. As a result, the mathematical formulation becomes impossible. The liquid jet is assumed to move axially while the airflow has both axial and tangential velocity components. The air swirl profiles considered in the study include the free vortex and the solid-body rotation. To compare the effectiveness of the two swirl profiles in stabilizing or destabilizing the liquid jet, effects of the swirl distribution (global effect) and the slope of the swirl profile (local effect) are examined. Detailed mathematical formulations of the global and local effects are given in § 2.6.

### 2.1. *Linearized disturbance equations*

The governing equations for incompressible viscous fluid flows are written in vector form as

$$\nabla \cdot \boldsymbol{V} = 0, \tag{1}$$

$$\rho\left(\frac{\partial \boldsymbol{V}}{\partial t}+\boldsymbol{V}\cdot\nabla\boldsymbol{V}\right)=-\nabla p+\mu\nabla^2\boldsymbol{V}, \tag{2}$$

where $\boldsymbol{V}=(U,V,W)$ is the velocity vector, $\rho$ is fluid density, $t$ is time, $p$ is the static pressure, and $\mu$ is the fluid dynamic viscosity. To derive the linearized disturbance equations, velocity and pressure disturbances are superposed on their mean counterparts:

$$\boldsymbol{V}=\bar{\boldsymbol{V}}+\boldsymbol{v},\quad p=\bar{P}+p', \tag{3}$$

where $\boldsymbol{v}=(u,v,w)$; the overbar represents the assumed mean flow quantities and the prime indicates the disturbance. The disturbances are assumed to have the forms

$$(u,v,w,p')=(\hat{u}(r),\hat{v}(r),\hat{w}(r),\hat{p}(r))\mathrm{e}^{\mathrm{i}(kx+n\theta-\omega t)}, \tag{4}$$

where the caret indicates disturbance amplitude which is a function of $r$ only, $k$ is the axial wavenumber, $n$ is the azimuthal wavenumber, and $\omega$ is the frequency. For temporal instability analysis, the wavenumbers $k$ and $n$ are real while frequency $\omega$ is complex. The imaginary part of $\omega$ reflects the growth rate of a disturbance. The displacement disturbance at the liquid/gas interface is assumed to be

$$\eta(x,\theta,t)=\hat{\eta}\mathrm{e}^{\mathrm{i}(kx+n\theta-\omega t)}. \tag{5}$$

Substituting (3) into (1) and (2) and neglecting second-order terms, we obtain the linearized disturbance equations for the liquid phase in vector form:

$$\nabla\cdot\boldsymbol{v}=0, \tag{6}$$

$$\rho_l\left(\frac{\partial \boldsymbol{v}}{\partial t}+U_l\frac{\partial \boldsymbol{v}}{\partial x}\right)=-\nabla p_l'+\mu\nabla^2\boldsymbol{v}, \tag{7}$$

In the case of the free-vortex swirl profile, the linearized disturbance equations for the gas phase can be written in component form as

$$\frac{\partial u}{\partial t}+\frac{A}{r^2}\frac{\partial u}{\partial\theta}+U_g\frac{\partial u}{\partial x}=-\frac{1}{\rho_g}\frac{\partial p_g'}{\partial x}, \tag{8}$$

$$\frac{\partial v}{\partial t}+U_g\frac{\partial v}{\partial x}+\frac{A}{r^2}\frac{\partial v}{\partial\theta}-\frac{2Aw}{r^2}=-\frac{1}{\rho_g}\frac{\partial p_g'}{\partial r}, \tag{9}$$

$$\frac{\partial w}{\partial t}+U_g\frac{\partial w}{\partial x}+\frac{A}{r^2}\frac{\partial w}{\partial\theta}=-\frac{1}{\rho_g}\frac{\partial p_g'}{r\partial\theta}, \tag{10}$$

where $A$ is the vortex strength and subscript $g$ represents the gas phase. Similarly, for the case of the solid-body-rotation profile, the linearized disturbance equations are governed by

$$\frac{\partial u}{\partial t}+\Omega\frac{\partial u}{\partial\theta}+U_g\frac{\partial u}{\partial x}=-\frac{1}{\rho_g}\frac{\partial p_g'}{\partial x}, \tag{11}$$

$$\frac{\partial v}{\partial t}+\Omega\frac{\partial v}{\partial\theta}+U_g\frac{\partial v}{\partial x}-2\Omega w=-\frac{1}{\rho_g}\frac{\partial p_g'}{\partial r}, \tag{12}$$

$$\frac{\partial w}{\partial t}+\Omega\frac{\partial w}{\partial\theta}+U_g\frac{\partial w}{\partial x}+2\Omega v=-\frac{1}{\rho_g}\frac{\partial p_g'}{r\partial\theta}, \tag{13}$$

where $\Omega$ is the angular velocity.

### 2.2. *Boundary conditions*

Boundary conditions must be prescribed at the jet surface to derive the dispersion equation. The kinematic boundary condition requires that the radial velocity component be continuous across the interface. The kinematic boundary condition for the liquid phase is given by

$$v = \frac{\mathrm{D}\eta}{\mathrm{D}t} = \frac{\partial \eta}{\partial t} + U_l \frac{\partial \eta}{\partial x} \quad \text{at} \quad r = a, \tag{14}$$

where $a$ is the jet radius. For the ambient air, the kinematic boundary conditions corresponding to the free-vortex and solid-body rotation profiles are, respectively,

$$v = \frac{\mathrm{D}\eta}{\mathrm{D}t} = \frac{\partial \eta}{\partial t} + \frac{A}{r^2}\frac{\partial \eta}{\partial \theta} + U_g \frac{\partial \eta}{\partial x} \quad \text{at} \quad r = a, \tag{15}$$

$$v = \frac{\mathrm{D}\eta}{\mathrm{D}t} = \frac{\partial \eta}{\partial t} + \Omega \frac{\partial \eta}{\partial \theta} + U_g \frac{\partial \eta}{\partial x} \quad \text{at} \quad r = a. \tag{16}$$

The dynamic boundary conditions in the axial, azimuthal, and radial directions are

$$\tau_{rx} = \mu \left( \frac{\partial u}{\partial r} + \frac{\partial v}{\partial x} \right) = 0, \tag{17}$$

$$\tau_{r\theta} = \mu \left( \frac{\partial w}{\partial r} + \frac{1}{r}\frac{\partial v}{\partial \theta} - \frac{w}{r} \right) = 0, \tag{18}$$

$$p_l' - p_g' = -\sigma \left( \frac{\eta}{a^2} + \frac{1}{a^2}\frac{\partial^2 \eta}{\partial \theta^2} + \frac{\partial^2 \eta}{\partial x^2} \right) + \frac{\rho_g A^2 \eta}{a^3} + 2\mu \frac{\partial v}{\partial r}, \tag{19}$$

$$p_l' - p_g' = -\sigma \left( \frac{\eta}{a^2} + \frac{1}{a^2}\frac{\partial^2 \eta}{\partial \theta^2} + \frac{\partial^2 \eta}{\partial x^2} \right) + \rho_g \Omega^2 a \eta + 2\mu \frac{\partial v}{\partial r}, \tag{20}$$

where $\sigma$ is the surface tension. Note that (19) and (20) correspond to the free-vortex and solid-body rotation profiles, respectively.

### 2.3. *Pressure disturbance in the liquid jet*

Taking the divergence of (7) and making use of (6) leads to

$$\nabla^2 p_l' = 0. \tag{21}$$

Substituting (4) into (21), we obtain the bounded solution for the amplitude of the pressure disturbance in the liquid as

$$\hat{p}_l(r) = -\rho_l(-\mathrm{i}\omega + \mathrm{i}kU_l) C_1 I_n(k\,r), \tag{22}$$

where $I_n$ is the $n$th-order modified Bessel function of the first kind. Upon substitution of (4) into (7) and transforming variables $(\hat{u}, \hat{v}, \hat{w})$ into $(\hat{u}_1, \hat{v}_1, \hat{w}_1)$ through the following relationships:

$$\hat{u}_1 = \hat{u} + \frac{1}{\rho_l(-\mathrm{i}\omega + \mathrm{i}kU_l)} \mathrm{i}k\hat{p}, \tag{23}$$

$$\hat{v}_1 = \hat{v} + \frac{1}{\rho_l(-\mathrm{i}\omega + \mathrm{i}kU_l)} \frac{\mathrm{d}\hat{p}}{\mathrm{d}r}, \tag{24}$$

$$\hat{w}_1 = \hat{w} + \frac{1}{\rho_l(-\mathrm{i}\omega + \mathrm{i}kU_l)} \frac{\mathrm{i}n}{r} \hat{p}, \tag{25}$$

we arrive at the following equations which govern the amplitudes of velocity disturbances:

$$\frac{\mathrm{d}^2\hat{u}_1}{\mathrm{d}r^2} + \frac{1}{r}\frac{\mathrm{d}\hat{u}_1}{\mathrm{d}r} - \frac{1}{r^2}(n^2 + s^2r^2)\hat{u}_1 = 0, \tag{26}$$

$$(B_n - 1)\hat{v}_1 = 2ni\hat{w}_1, \tag{27}$$

$$(B_n - 1)\hat{w}_1 = -2ni\hat{v}_1, \tag{28}$$

where

$$s^2 = k^2 + \frac{(-\mathrm{i}\omega + \mathrm{i}kU_l)}{v}$$

and the Bessel operator $B_n$ is given by

$$B_n = r^2\frac{\mathrm{d}^2}{\mathrm{d}r^2} + r\frac{\mathrm{d}}{\mathrm{d}r} - (n^2 + s^2r^2).$$

Solutions to (26), (27) and (28) are, respectively,

$$\hat{u}_1 = C_2 I_n(sr), \tag{29}$$

$$\hat{v}_1 = C_3 I_{n-1}(s\,r) + C_4 I_{n+1}(s\,r), \tag{30}$$

$$\hat{w}_1 = \mathrm{i}(C_3 I_{n-1}(s\,r) - C_4 I_{n+1}(s\,r)). \tag{31}$$

Substituting (23), (24), (25), (29), (30) and (31) into (6) leads to the relationship among $C_2, C_3$ and $C_4$ as follows:

$$C_3 = -\frac{\mathrm{i}kC_2}{s} - C_4. \tag{32}$$

Hence, the amplitudes of velocity disturbances in the liquid phase can be expressed by

$$\hat{u} = \mathrm{i}kC_1 I_n(k\,r) + C_2 I_n(s\,r), \tag{33}$$

$$\hat{v} = kC_1 I_n'(k\,r) - \frac{\mathrm{i}k}{s}C_2 I_{n-1}(s\,r) + \frac{n}{s\,r}C_5 I_n(s\,r), \tag{34}$$

$$\hat{w} = \mathrm{i}\left[\frac{nC_1}{r}I_n(k\,r) - \frac{\mathrm{i}k}{s}C_2 I_{n-1}(s\,r) + C_5 I_n'(s\,r)\right], \tag{35}$$

where $C_5 = -2C_4$. Constants $C_1, C_2$ and $C_5$ are determined by utilizing boundary conditions, i.e. (14), (17) and (18). Their expressions are given in Liao (1999) and are not repeated here for brevity. The final form of the pressure disturbance inside the liquid jet can be expressed as

$$p_l' = -\rho_l(-\mathrm{i}\omega + \mathrm{i}kU_l)^2\hat{\eta}\frac{J_1}{J_2}\frac{aI_n(k\,r)}{I_n(ka)}\mathrm{e}^{\mathrm{i}(kx+n\theta-\omega t)}, \tag{36}$$

where

$$J_1 = \frac{(ka)^2}{(sa)^2}n\left[saI_{n-1}'(sa) - I_{n-1}(sa)\right] + \frac{n^2(ka)^2}{(sa)^2}\frac{I_{n-1}(sa)}{I_n'(sa)}$$

$$-\frac{1}{I_n(sa)}\left[(sa)^2 I_n''(sa) - saI_n'(sa) + n^2 I_n(sa)\right]\left(\frac{k^2}{s^2}\frac{I_{n-1}(sa)}{I_n'(sa)} + 1\right), \tag{37}$$

$$J_2 = 2n^2\left[\frac{kaI_n'(ka)}{I_n(ka)} - 1\right] - \frac{n^2(ka)^2}{(sa)^2}\frac{kaI_n'(ka)}{I_n(ka)}\frac{I_{n-1}(sa)}{I_n'(sa)} - \frac{(ka)^3}{(sa)^2}\frac{I_n'(ka)}{I_n'(sa)}\frac{n}{I_n(ka)}\left[saI_{n-1}'(sa) - I_{n-1}(sa)\right] - \frac{kaI_n'(ka)}{I_n(ka)} \times \left[(sa)^2\frac{I_n''(sa)}{I_n(sa)} - sa\frac{I_n'(sa)}{I_n(sa)} + n^2\right]\left(\frac{k^2}{s^2}\frac{I_{n-1}(sa)}{I_n'(sa)} - 1\right). \tag{38}$$

### 2.4. *Pressure disturbance in the swirling air*

In the case of the free-vortex swirl profile, substitution of (4) into (6), (8), (9) and (10) leads to

$$\hat{w} = \frac{n}{kr}\hat{u}, \tag{39}$$

$$\hat{v} = -\frac{\mathrm{i}}{k}\frac{\mathrm{d}\hat{u}}{\mathrm{d}r}. \tag{40}$$

Therefore, the continuity equation can be rewritten as

$$\frac{\mathrm{d}^2\hat{u}}{\mathrm{d}r^2} + \frac{1}{r}\frac{\mathrm{d}\hat{u}}{\mathrm{d}r} - \left(\frac{n^2}{r^2} + k^2\right)\hat{u} = 0. \tag{41}$$

The above equation is a modified Bessel equation with a bounded solution in the form of

$$\hat{u}(r) = C_6K_n(kr), \tag{42}$$

where $K_n$ is the $n$th-order Bessel function of the second kind. The pressure disturbance inside the gas phase is given by, after constant $C_6$ is determined from (15),

$$p_g' = \frac{\rho_g}{k}\left(-\omega + \frac{An}{a^2} + kU_g\right)\left(-\omega + \frac{An}{r^2} + kU_g\right)\hat{\eta}\frac{K_n(kr)}{K_n'(ka)}\mathrm{e}^{\mathrm{i}(kx+n\theta-\omega t)}. \tag{43}$$

In a similar fashion, for the case of the solid-body-rotation profile, $\hat{v}$ and $\hat{w}$ are expressed as

$$\hat{v} = \frac{-\mathrm{i}\left[(-\omega + n\Omega + kU_i)^2\frac{\mathrm{d}\hat{u}}{\mathrm{d}r} + \frac{2n\Omega}{r}(-\omega + n\Omega + kU_i)\hat{u}\right]}{k[(-\omega + n\Omega + kU_i)^2 - 4\Omega^2]}, \tag{44}$$

$$\hat{w} = \frac{\left[(-\omega + n\Omega + kU_i)^2\hat{u} + 2\Omega(-\omega + n\Omega + kU_i)\frac{\mathrm{d}\hat{u}}{\mathrm{d}r}\right]}{k[(-\omega + n\Omega + kU_i)^2 - 4\Omega^2]}. \tag{45}$$

And the continuity equation can be rewritten in the form

$$\frac{\mathrm{d}^2\hat{u}}{\mathrm{d}r^2} + \frac{1}{r}\frac{\mathrm{d}\hat{u}}{\mathrm{d}r} - \frac{1}{r^2}\left[n^2 + k^2r^2\left(1 - \frac{4\Omega^2}{(-\omega + n\Omega + kU_g)^2}\right)\right]\hat{u} = 0. \tag{46}$$

The bounded solution to the above equation is

$$\hat{u}(r) = C_7K_n\left(kr\sqrt{1 - \frac{4\Omega^2}{(-\omega + n\Omega + kU_g)^2}}\right). \tag{47}$$

Therefore, in the case of the solid-body-rotation profile, after constant $C_7$ is determined

from (16), the pressure disturbance in the gas phase can be expressed as

$$p'_g = \frac{\rho_g[(-\omega + n\Omega + kU_g)^2 - 4\Omega^2](-\omega + n\Omega + kU_g)\hat{\eta}K_n(k_1 r)}{(2n\Omega/a)K_n(k_1 a) + (-\omega + n\Omega + kU_g)k_1 K'_n(k_1 a)} e^{i(kx+n\theta-\omega t)}, \tag{48}$$

where $k_1 = k\sqrt{1 - \dfrac{4\Omega^2}{(-\omega + n\Omega + kU_g)^2}}$.

### 2.5. *Dispersion equations*

The dispersion equation is obtained by means of substitution of the pressure disturbances ((36), (43) or (48)) inside the liquid and gas phases into the dynamic boundary condition ((19) or (20)). To isolate the effects of flow conditions as well as fluid properties on the instability of the liquid jet, the dispersion equation is non-dimensionalized by introducing the following dimensionless parameters:

$$\left.\begin{aligned} &We_l = \frac{\rho_l U_l^2 a}{\sigma}, \quad We_s = \frac{\rho_l W^2 a}{\sigma}, \quad We_{sf} = \frac{\rho_l A^2}{\sigma a}, \quad We_{ss} = \frac{\rho_l \Omega^2 a^3}{\sigma}, \quad U_r = \frac{U_g}{U_l}, \\ &\bar{\rho} = \frac{\rho_g}{\rho_l}, \quad Z = \frac{\mu}{(\rho_l \sigma a)^{1/2}}, \quad \bar{k} = ka, \quad \bar{s} = sa, \quad \bar{\omega} = \frac{\omega}{(\sigma/\rho_l a^3)^{1/2}}. \end{aligned}\right\} \tag{49}$$

The non-dimensional dispersion equations corresponding to the free-vortex and solid-body rotation profiles are, respectively,

$$\begin{aligned} &(-\bar{\omega} + \bar{k}We_l^{1/2})^2 \frac{J_1}{J_2} - \frac{\bar{\rho}K_n(\bar{k})}{\bar{k}K'_n(\bar{k})}(-\bar{\omega} + nWe_{sf}^{1/2} + \bar{k}U_r We_l^{1/2})^2 \\ &\quad -2Z(-\bar{\omega} + \bar{k}We_l^{1/2})\left\{\frac{\bar{k}^2 I''_n(\bar{k})}{I_n(\bar{k})}\frac{J_1}{J_2} - \frac{\bar{k}^2}{\bar{s}}\frac{I'_{n-1}(\bar{s})}{I'_n(\bar{s})}\left(\frac{\bar{k}I'_n(\bar{k})}{I_n(\bar{k})}\frac{J_1}{J_2}\right)\right. \\ &\quad \left. + \frac{\bar{s}I'_n(\bar{s}) - I_n(\bar{s})}{I_n(\bar{s})}\left[-\frac{\bar{k}I'_n(\bar{k})}{I_n(\bar{k})}\frac{J_1}{J_2} + \frac{\bar{k}^2 I_{n-1}(\bar{s})}{\bar{s}^2 I'_n(\bar{s})}\left(1 + \frac{\bar{k}I'_n(\bar{k})}{I_n(\bar{k})}\frac{J_1}{J_2}\right) + 1\right]\right\} \\ &\quad = -(1 - \bar{k}^2 + n^2) + \bar{\rho}We_{sf}, \end{aligned} \tag{50}$$

$$\begin{aligned} &(-\bar{\omega} + \bar{k}We_l^{1/2})^2 \frac{J_1}{J_2} - \frac{\bar{\rho}[\bar{\omega}_1^2 - 4We_{ss}]\bar{\omega}_1 K_n(\bar{k}_1)}{2nWe_{ss}^{1/2}K_n(\bar{k}_1) + \bar{k}_1\bar{\omega}_1 K'_n(\bar{k}_1)} \\ &\quad -2Z(-\bar{\omega} + \bar{k}We_l^{1/2})\left\{\frac{\bar{k}^2 I''_n(\bar{k})}{I_n(\bar{k})}\frac{J_1}{J_2} - \frac{\bar{k}^2}{\bar{s}}\frac{I'_{n-1}(\bar{s})}{I'_n(\bar{s})}\left(\frac{\bar{k}I'_n(\bar{k})}{I_n(\bar{k})}\frac{J_1}{J_2} + 1\right)\right. \\ &\quad \left. + \frac{\bar{s}I'_n(\bar{s}) - I_n(\bar{s})}{I_n(\bar{s})}\left[-\frac{\bar{k}I'_n(\bar{k})}{I_n(\bar{k})}\frac{J_1}{J_2} + \frac{\bar{k}^2 I_{n-1}(\bar{s})}{\bar{s}^2 I'_n(\bar{s})}\left(1 + \frac{\bar{k}I'_n(\bar{k})}{I_n(\bar{k})}\frac{J_1}{J_2}\right) + 1\right]\right\} \\ &\quad = -(1 - \bar{k}^2 + n^2) + \bar{\rho}We_{ss}, \end{aligned} \tag{51}$$

where $\bar{k}_1 = \bar{k}\sqrt{1 - \dfrac{4We_{ss}}{(-\bar{\omega} + nWe_{ss}^{1/2} + \bar{k}U_r We_l^{1/2})^2}}$, $\quad \bar{\omega}_1 = (-\bar{\omega} + nWe_{ss}^{1/2} + \bar{k}U_r We_l^{1/2})$.

Equations (50) and (51) do not have closed-form solutions. They were numerically solved using the secant method, which requires two guessed complex values. For a swirling case, solutions of its non-swirling counterpart were taken as the guessed values. The solution was considered converged when the value of left-hand side of the dispersion equation was smaller than $10^{-8}$. For each pair of $(\bar{k}, n)$ and given

dimensionless parameters, we solved for the root with the maximum imaginary part, which represents the growth rate of a disturbance.

### 2.6. *Global and local effect*

It is well known that the hydrodynamic stability of a fluid flow depends upon its velocity profile, and the instability of a liquid jet is controlled by the fluctuating pressure difference between the liquid and gas phases. For a given airflow moving with a uniform axial velocity component, the radial pressure gradient is determined by its swirling component. Therefore, the air swirl profile is expected to have a significant effect on the instability of the liquid jet. For the two profiles chosen, a fundamental question arises as to which profile – the free vortex or solid-body rotation – has a more significant effect on the instability of the liquid jet? To answer this question, the concepts of global and local effects are defined and formulated below.

The global effect refers to the effect of air swirl distribution on the instability of the liquid jet. That is, for an equal amount of angular momentum distributed within a thin layer near the interface ($r = a$), which profile, the free vortex or solid-body rotation, affects the flow more significantly? The angular momentum $G_\theta$ in a thin layer of a thickness of ($b$-$a$) can be expressed as

$$G_\theta = \int_a^b (Wr)\rho U 2\pi r \mathrm{d}r. \tag{52}$$

For the two swirl profiles, as shown in figure 2($a$), an equal amount of angular momentum within a layer of thickness $a(b = 2a)$ leads to

$$\Omega = \frac{2A}{5a^2}. \tag{53}$$

The local effect refers to the effect of the slope of a swirl profile at the jet surface on the instability of the liquid jet. It can be shown that for equal tangential velocity at the jet surface, the free-vortex and solid-body-rotation profiles have equal slopes but with opposite sign as shown in figure 2($b$). As the swirl Weber number for the free-vortex and the solid-body-rotation profiles have been defined as $We_{sf} = \rho_l A^2/\sigma a$ and $We_{ss} = \rho_l \Omega^2 a^3/\sigma$, for a given nozzle geometry and fluid properties, the swirl Weber number thus reflects the local effect. Given a swirl Weber number, the local effect can be clearly understood by comparing the growth rates of various modes corresponding to the free-vortex and solid-body-rotation profiles.

## 3. Results and discussion

A comprehensive parametric study has been conducted to investigate the effects of flow parameters and fluid properties on the instability of a liquid jet. The parameter space consists of the axial Weber number, $We_l$, the velocity ratio of gas to liquid, $U_r$, the swirl Weber numbers, $We_s$, $We_{sf}$ and $We_{ss}$, gas-to-liquid density ratio, $\bar{\rho}$, and Ohnesorge number, $Z$. An extensive effort has been made towards the understanding of the effects of air swirl and swirl profile on the instability of the liquid jet. Both qualitative and quantitative comparisons have been made between the theoretical predictions and available experimental data, and agreement is very good.

### 3.1. *Model validation*

To validate our theoretical model, we first consider the limiting case of a jet discharging in stagnant air. Figures 3($a$), 3($b$) and 3($c$) show the growth rates of unstable waves

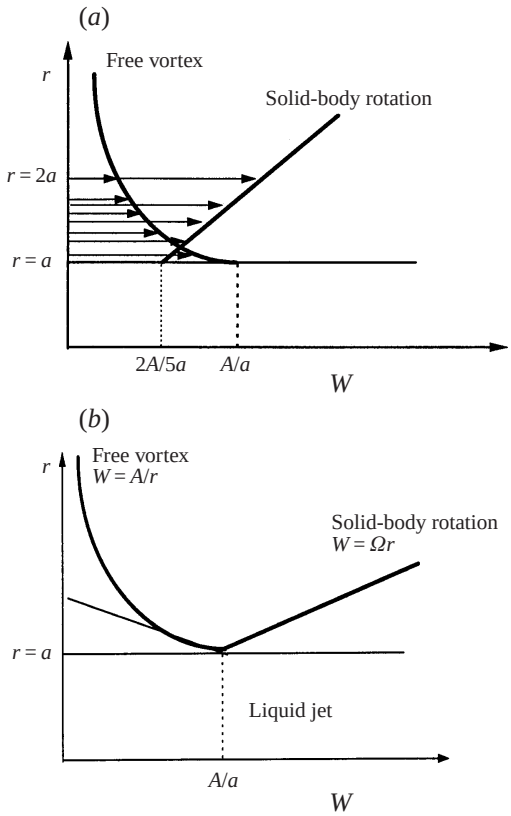


FIGURE 2. (*a*) Swirl distribution within a layer of thickness of *a*, and (*b*) equal tangential velocity leads to equal slope of swirl profile at the jet surface.

versus axial Weber number in the Rayleigh, the first wind-induced and the second wind-induced regimes, respectively. It should be noted that the current stability model could not distinguish the second wind-induced regime from the atomization regime. As can be clearly seen from the figures, at each axial Weber number, there exists a finite range of wavenumbers, $\bar{k}$, where the growth rates are positive. Also, there is a wavenumber that corresponds to the maximum growth rate $\bar{\omega}_{i\max}$. This wavenumber is called the most unstable wavenumber $\bar{k}_*$. It is also seen from figure 3(*a*), that at very low jet velocity the axisymmetric mode ($n = 0$) has the highest growth rate within the entire unstable range and thus dominates the growth competition of unstable waves. This conclusion was proposed by Rayleigh and later validated by experiments (Lefebvre 1989). As jet velocity increases as shown in figure 3(*b*), the maximum growth rate and the most unstable wavenumber shift to higher values. More importantly, the growth rate of helical modes becomes comparable with that of the axisymmetric mode. In certain ranges of wavenumbers, their growth rates are higher than that of the axisymmetric mode. This behaviour has also been observed in several experimental studies (Hoyt & Taylor 1977; Chigier 1989; Krulle *et al.* 1990). To further compare the predicted trend of breakup length with observed behaviour, variations of the maximum growth rate and the most unstable wavenumber with axial Weber number have been correlated for the first and second wind-induced regimes (Liao *et al.* 1998). It was shown that the stability model correctly predicts the trend of the variation of intact length with jet velocity in all three regimes.

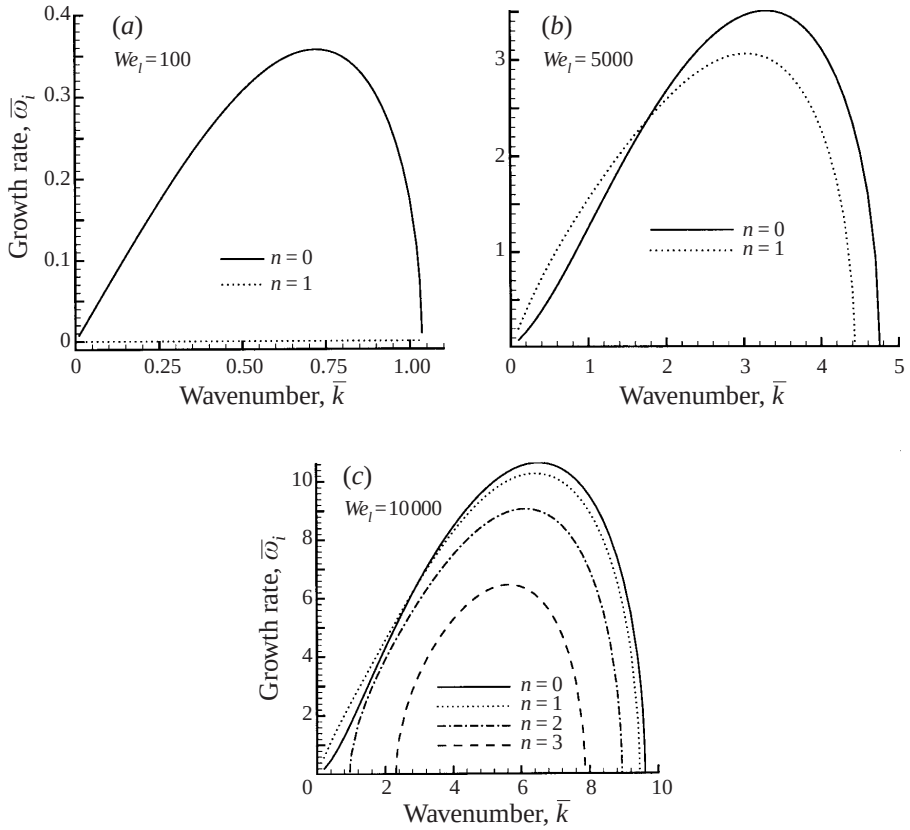


FIGURE 3. Non-dimensional growth rates versus wavenumber in three regimes: (*a*) Rayleigh regime, (*b*) first wind-induced regime, and (*c*) second wind-induced regime. $We_s = 0$, $U_r = 0$, $\bar{\rho} = 0.001$, $Z = 0.001$.

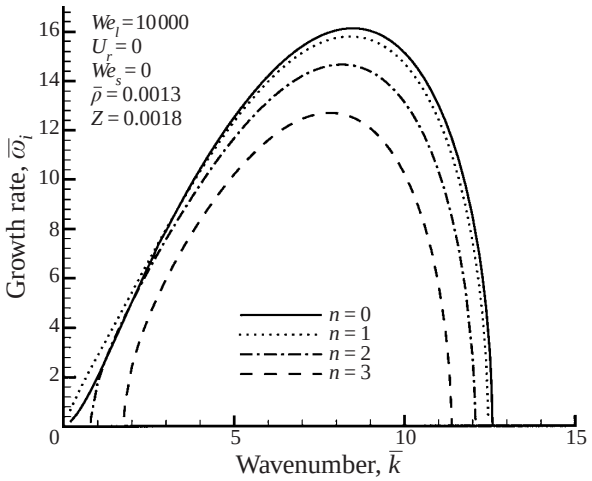


FIGURE 4. Predicted non-dimensional growth rate versus wavenumber with the same flow conditions and fluid properties as Hoyt & Taylor's (1977) experiment.

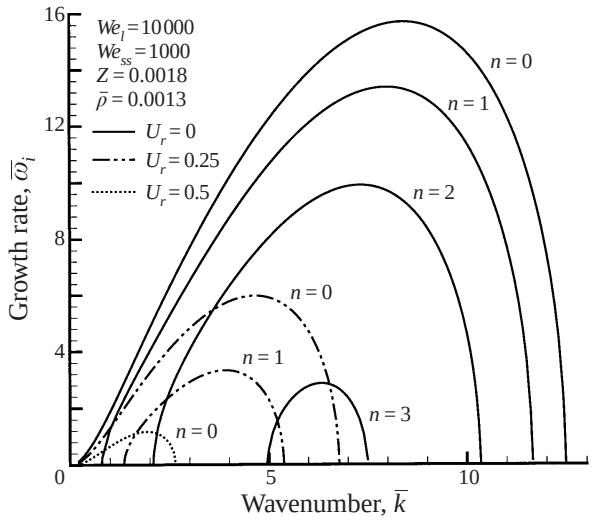


FIGURE 5. Effect of relative axial velocity between the liquid and gas phases on the instability of the liquid jet.

To quantitatively validate the stability model with experimental data, values of flow parameters and fluid properties are chosen to be the same as those of Case 2 listed in Table I of Yang (1992). Figure 4 shows that the first helical mode ($n = 1$) indeed has the highest growth rate among all modes in the range $0 < \bar{k} < 3.2$, which is close to the experimental result of $0 < \bar{k} < 1.75$. Improvement is evident when compared with Yang's inviscid prediction of $0 < \bar{k} < 3.5$.

In summary, our results in the limit of zero air velocity have been extensively validated and agree well with earlier theoretical and experimental studies. Results of a liquid jet subjected to air moving with both axial and swirling velocity components are discussed below.

### 3.2. *Effect of relative axial velocity*

The effect of the relative axial velocity between the liquid jet and the ambient air is investigated by considering the axial velocity ratio of gas to liquid, $U_r$. Figure 5 illustrates this effect on the growth rates of various unstable modes when the ambient air is swirling with a solid-body-rotation profile. For a given jet velocity, as the axial component of air velocity is increased, i.e. as the relative axial velocity is decreased, the growth rate and the most unstable wavenumber shift to lower values thus making the jet more stable. This confirms that it is the relative axial velocity between the liquid jet and the gas that determines the instability of the liquid jet. The above statement can be explained in terms of aerodynamic interaction between the liquid and gas phases. The difference between the fluctuating pressures in the liquid and gas phases reflects the strength of aerodynamic interaction and causes the breakup of the liquid jet. The smaller the relative velocity is, the smaller the fluctuating pressure difference, and hence the weaker the aerodynamic interaction. Thus, the jet becomes more stable.

### 3.3. *Effect of fluid properties*

The influence of gas-to-liquid density ratio on the instability of the liquid jet is shown in figure 6, where the solid line represents the non-swirling flow condition and the

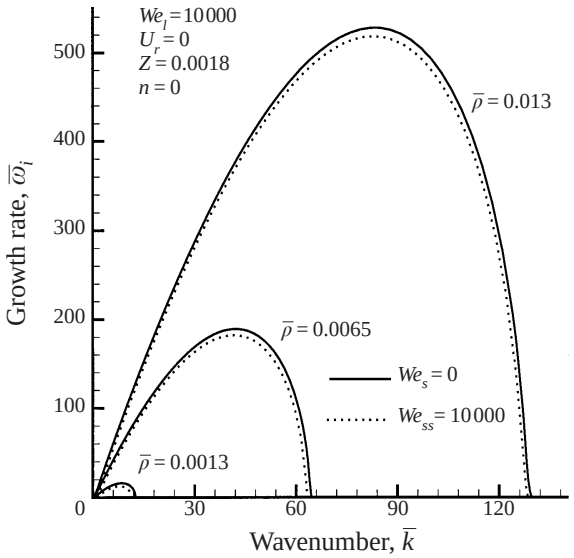


FIGURE 6. Effect of density ratio on growth rates of unstable waves.

dotted line corresponds to the swirling case. For both flow conditions, it is evident that the most unstable wavenumber, the unstable range, and the maximum growth rate increase with increasing gas density. Since an increase in gas density increases the aerodynamic force, it enhances the aerodynamic interaction between the liquid and gas phase as expected. As droplet sizes and breakup length are related to the wavelength of the most unstable waves and the maximum growth rate, respectively, a high gas/liquid density ratio thus leads to smaller droplets and a shorter breakup length. This conclusion is in agreement with results reported in the literature (Lefebvre 1989). Ranze (1958) further argued that jet spray angle can be estimated from the ratio of the disturbance amplitude increase to the distance travelled by the fluid particle in the same time period. According to this argument, for a given jet velocity, a higher growth rate implies a larger spray angle. Hence, the results of the linear stability analysis indicate that spray angle increases with density ratio. This trend is consistent with extensive experimental data reported by Reitz & Bracco (1982). Furthermore, it is interesting to note that the effect of the density ratio on the growth rate is almost comparable to that of the axial Weber number. For example, a ten-fold increase in density ratio increases the maximum growth rate by 33 times, while a ten-fold increase in axial Weber number increases the maximum growth rate by 34 times. This observation is consistent with available empirical correlations for the intact length and mean droplet size, in which the axial Weber number and density ratio are raised to the same power (Bayvel & Orzechowski 1993). It may be noted that the effect of density ratio on jet instability may not be the same in all regimes. In the Rayleigh regime, the density ratio has been shown to exhibit a stabilizing effect on the liquid jet (Li & Shen 1998). In this regime, the liquid Weber number is smaller than the critical Weber number and the liquid jet is absolutely unstable, which is caused by surface tension.

Figure 7 illustrates the effect of viscosity on the growth rates of both the axisymmetric and helical modes. It is clearly seen that liquid viscosity inhibits the growth of unstable waves and shifts the most unstable wavenumber to a lower value for both

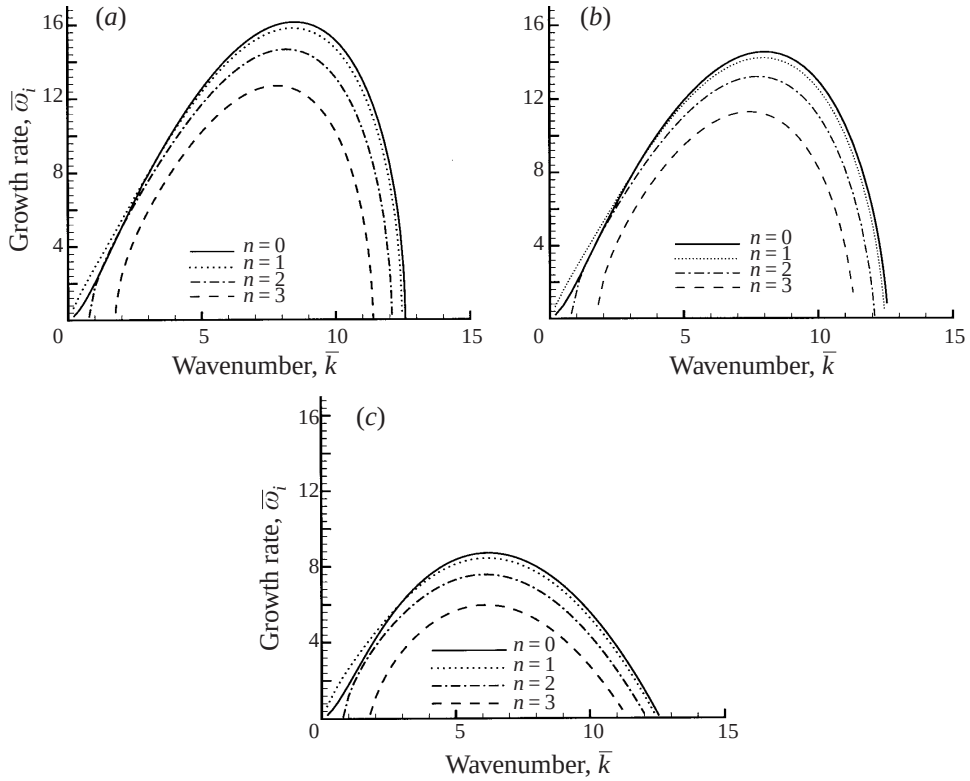


FIGURE 7. Effect of viscosity on the growth rates of axisymmetric and helical modes: (*a*) $Z = 0.0018$; (*b*) $Z = 0.018$; (*c*) $Z = 0.18$. $We_l = 10\,000$, $U_r = 0$, $We_s = 0$, $\bar{\rho} = 0.0013$.

the axisymmetric and helical modes. This implies that a high value of liquid viscosity delays the breakup of the liquid jet and results in a longer intact length, smaller spray angle and larger drop sizes. These results are also consistent with experimental observations (Reitz & Bracco 1982; Lefebvre 1989). However, the liquid viscosity does not change the unstable range of wavenumbers, as demonstrated by Chandrasekhar (1961).

An important question remains to be answered: which mode, the axisymmetric mode or helical mode, does liquid viscosity damp more significantly? To answer this question, a concept called 'relative importance' of a helical mode compared with the axisymmetric mode is defined as the ratio of the maximum growth rate of a helical mode to that of the axisymmetric mode, i.e. $(\bar{\omega}_{i\max})_n/(\bar{\omega}_{i\max})_0$. Table 1 lists the values of 'relative importance' for the first three helical modes at three different Ohnesorge numbers. Table 1 indicates that as the Ohnesorge number (liquid viscosity) increases, the relative importance of helical modes decreases. The highest helical mode has the most significant decrease. Therefore, viscosity damps the higher helical modes most. This theory helps to explain why only the axisymmetric mode and lower helical modes, instead of higher helical modes, are typically observed in experiments. It also demonstrates why the effect of liquid viscosity must be considered in the establishment of accurate correlations for the maximum growth rate and the corresponding wavelength, as was done by Reitz (1987).

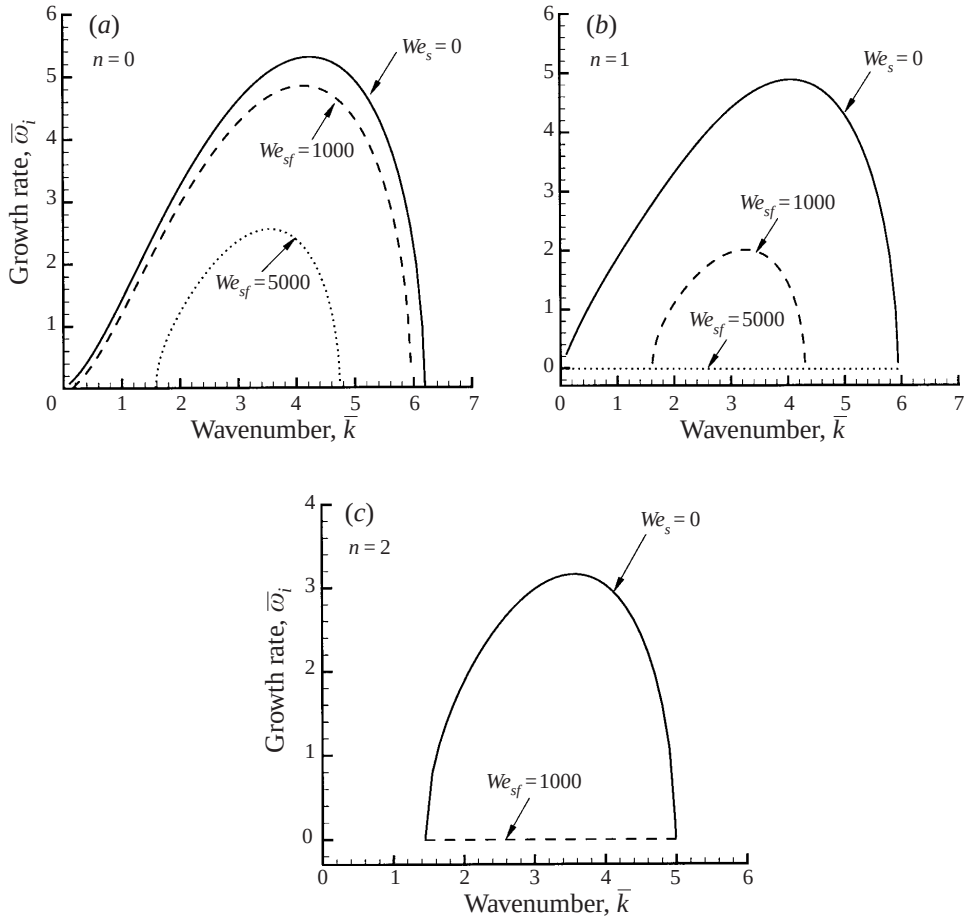


FIGURE 8. Effect of air swirl on the growth rates of the axisymmetric and helical modes: (*a*) $We_s = 0$; (*b*) $We_s = 1000$; (*c*) $We_s = 5000$. $We_l = 5000$, $U_r = 0$, $Z = 0.0018$, $\bar{\rho} = 0.0013$.

| | $Z = 0.0018$ | | $Z = 0.018$ | | $Z = 0.18$ | |
|---|---|---|---|---|---|---|
| mode | $\dfrac{(\bar{\omega}_{i\max})_n}{(\bar{\omega}_{i\max})_0}$ | $\bar{\omega}_{i\max}$ | $\dfrac{(\bar{\omega}_{i\max})_n}{(\bar{\omega}_{i\max})_0}$ | $\bar{\omega}_{i\max}$ | $\dfrac{(\bar{\omega}_{i\max})_n}{(\bar{\omega}_{i\max})_0}$ | $\bar{\omega}_{i\max}$ |
| $n = 0$ | 1.0000 | 16.127 | 1.0000 | 14.539 | 1.0000 | 8.702 |
| $n = 1$ | 0.9785 | 15.780 | 0.9778 | 14.216 | 0.9688 | 8.431 |
| $n = 2$ | 0.9087 | 14.654 | 0.9075 | 13.194 | 0.8690 | 7.562 |
| $n = 3$ | 0.7878 | 12.692 | 0.7757 | 11.279 | 0.6845 | 5.957 |

TABLE 1. Effect of Ohnesorge number on $(\bar{\omega}_{i\max})_n/(\bar{\omega}_{i\max})_0$.

### 3.4. *Effect of air swirl*

The effects of air swirl on the growth rates of the axisymmetric and helical modes are illustrated in figure 8. It is clearly seen that, with a free-vortex swirl profile, as the swirl strength increases, the growth rate and the most unstable wavenumber of the axisymmetric mode decrease. Moreover, the growth rates of helical modes are reduced

more significantly than that of the axisymmetric mode. Therefore, the axisymmetric mode becomes the dominant mode in the breakup of the liquid jet as swirl is added to the ambient air. In contrast, for an annular liquid sheet, liquid as well as air swirl enhance the helical modes more significantly than the axisymmetric mode, thus making higher helical modes dominant (Liao *et al.* 1999*a*, *b*). The fact that air swirl inhibits the atomization process of the liquid jet has also been observed in previous studies (Lian & Lin 1990; Ramamurthi & Madhavan 1998). This behaviour can be explained as follows. Inside the swirling air, there exists a pressure gradient, leading to increasing air static pressure in the positive radial direction. As the liquid surface is disturbed outward into the swirling air stream, the increasing static pressure of the ambient air pushes the surface back towards the undisturbed position, thus making the liquid jet stable. This illustrates that the effect of swirling air is identical to that of surface tension beyond the Rayleigh regime: both damp out the small disturbances at the liquid/air interface.

Although it is evident from the above discussion that air swirl has a stabilizing effect on the instability of the liquid jet, the effect of air swirl profile still remains unclear. To study this effect, free-vortex and solid-body-rotation swirl profiles are considered. Growth rates corresponding to these two profiles are calculated and compared with their non-swirling counterparts. Local as well as global effects of the swirl profiles are quantitatively investigated.

As was discussed in § 2.6, the local effect is reflected by the slope of swirl profile at the jet surface or by the swirl Weber number. Figure 9 illustrates the local effect of swirl profile on the instability of the liquid jet. Growth rates of the axisymmetric mode corresponding to the free-vortex and solid-body-rotation profiles are compared with their non-swirling counterpart in figure 9(*a*). It is clearly seen that their growth rates are lower than their non-swirling counterpart. This demonstrates that air swirl indeed has a stabilizing effect on the liquid jet with both swirl profiles. However, with the same slope at the jet surface, the free-vortex swirl profile leads to higher growth rates than the solid-body-rotation profile. The stronger the air swirl, the larger the difference of growth rate between these two swirl profiles. Therefore, with regard to the local effect, the solid-body-rotation profile is more effective in stabilizing the liquid jet. This can be explained as follows. Equal slope of swirl profile leads to the same swirling velocity component at the jet surface. However, for a solid-body-rotation profile, the tangential velocity increases while that of the free-vortex profile decreases. Therefore, the pressure gradient associated with the solid-body-rotation profile is larger than that with free-vortex profile. This larger pressure gradient leads to a greater stabilizing effect on the liquid jet as discussed before. Comparing figures 9(*a*) and 9(*b*), we also note that the effect of air swirl on the growth rates of helical modes is more significant than on that of the axisymmetric mode.

The global effect of the swirl profile is examined by distributing an equal amount of angular momentum within a thin layer near the jet surface. Figures 10(*a*) and 10(*b*) are comparisons of growth rates of the axisymmetric ($n = 0$) and the first helical mode ($n = 1$) between the free-vortex and solid-body-rotation swirl profiles when an equal amount of angular momentum is distributed within a layer of thickness $a$. Again, we find that air swirl leads to lower growth rates than the non-swirling case and stabilizes the liquid jet. More importantly, with equal amounts of angular momentum, the solid-body-rotation profile has higher growth rates and larger values of the most unstable wavenumbers than the free-vortex swirl profile. Therefore, as far as the global effect is concerned, the free-vortex swirl profile is more effective in stabilizing the liquid jet, which is opposite to that associated with the local effect. This

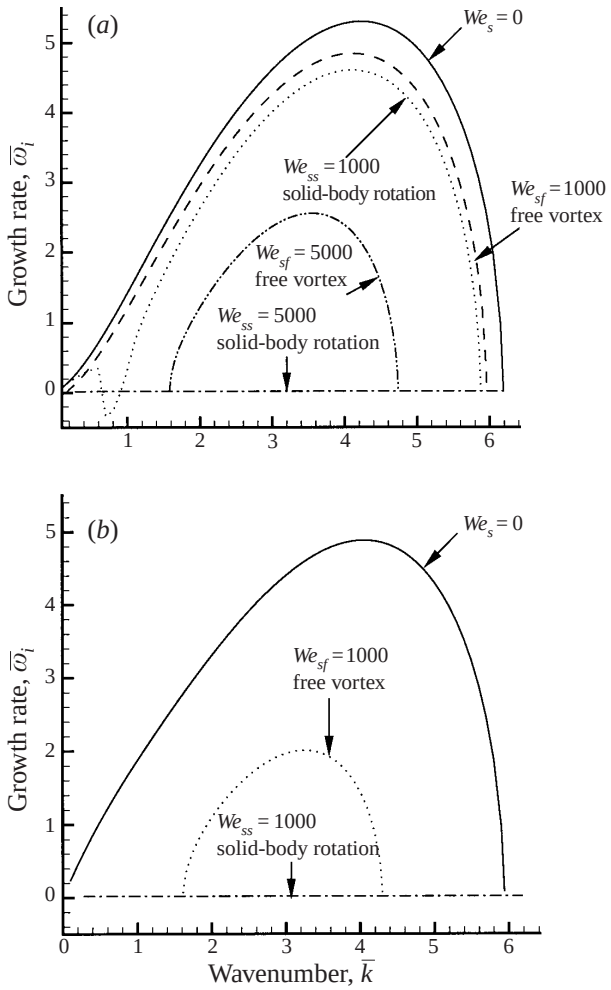


FIGURE 9. Local effect – comparison of growth rates of the axisymmetric and the first helical mode between free-vortex and solid-body-rotation swirl profile with equal slope at the jet surface: (*a*) $n = 0$ mode and (*b*) $n = 1$ mode. $We_l = 5000$, $U_r = 0$, $Z = 0.0018$, $\bar{\rho} = 0.0013$.

behaviour can be explained by considering figure 2(*a*), which shows that the tangential velocity with the free-vortex profile is larger than that with solid-body-rotation profile near the jet surface. This leads to a larger static air pressure in the vicinity of jet surface. Therefore, the free-vortex swirl profile becomes more effective in stabilizing the liquid jet.

In summary, the air swirl profile has a significant effect on the instability of the liquid jet. With equal slope of swirl profile, the solid-body-rotation profile is more effective in stabilizing the liquid jet than the free-vortex profile. However, when equal amounts of angular momentum are distributed within a thin layer, the free-vortex profile becomes more effective than solid-body rotation in stabilizing the liquid jet. It is the tangential velocity in the vicinity of the jet surface that determines the effectiveness of the swirl profile in stabilizing the liquid jet.

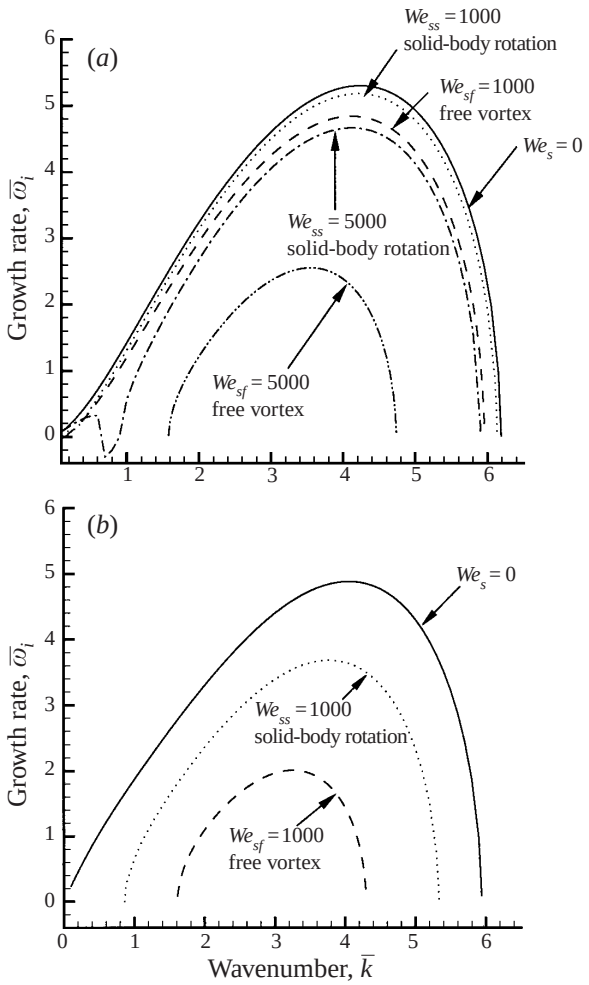


FIGURE 10. Global effect – comparison of growth rates between the free-vortex and solid-body-rotation profiles when layer thickness equals $a$: ($a$) $n = 0$ mode and ($b$) $n = 1$ mode. Same flow conditions as figure 9.

## 4. Conclusions

A theoretical model has been developed to predict the instability of a viscous liquid jet subjected to an air stream moving with both swirling and axial velocity components. It has been shown that results from earlier studies can be recovered by considering limiting cases of the present model. Effects of flow conditions (in terms of axial Weber number, velocity ratio, and swirl Weber number) and fluid properties (in terms of density ratio and Ohnesorge number) are investigated. From the study, we can draw the following conclusions:

(i) The relative axial velocity between the liquid and gas phases promotes jet instability whereas the liquid viscosity tends to stabilize the liquid jet. For the range of Weber numbers considered in this study, an increase in the gas-to-liquid density ratio increases the maximum growth rate and the most unstable wavenumber.

(ii) As the liquid axial Weber number increases, the importance of helical modes compared to that of the axisymmetric mode increases, resulting in a transition from

the Rayleigh regime to the first wind-induced regime and subsequently to the second wind-induced regime.

(iii) Liquid viscosity reduces the growth rates of unstable waves and damps the higher helical modes more significantly than the axisymmetric mode.

(iv) Both the free-vortex and the solid-body-rotation swirl profiles were found to exhibit a stabilizing effect on the liquid jet. With increasing air swirl strength, the growth rates for higher helical modes are reduced more significantly than the axisymmetric mode.

(v) With an equal slope of swirl profile (local effect) at the jet surface, the solid-body-rotation profile in more effective in stabilizing the liquid jet than a free-vortex profile. However, when equal amounts of angular momentum are distributed within a layer (global effect) in the vicinity of the interface, the free-vortex profile becomes more effective in stabilizing the jet than the solid-body-rotation profile.

(vi) It is the magnitude of the tangential velocity component in the vicinity of the jet surface that determines the effectiveness of air swirl profile in stabilizing the liquid jet.

Support for this work was provided by Parker Hannifin Corporation, National Science Foundation and NASA Glenn Research Center under grant NAG3-1987.

## REFERENCES

Bayvel, L. & Orzechowski, Z. 1993 *Liquid Atomization*. Taylor & Francis.

Chandrasekhar, S. 1961 *Hydrodynamic and Hydromagnetic Stability*. Oxford University Press.

Chigier, N. 1989 Atomization of liquid jets from injection element in liquid rocket combustion chamber. *Second Quarterly Report to NASA*.

Drazin, P. G. & Reid, W. H. 1985 *Hydrodynamic Stability*. Cambridge University Press.

Faeth, G. M., Hsiang, L. P. & Wu, P. K. 1995 Structure and breakup properties of sprays. *Intl J. Multiphase Flow* **21**, Supplement 99–127.

Heywood, J. B. 1988 *Internal Combustion Engine Fundamentals*. McGraw-Hill.

Hoyt, J. W. & Taylor J. J. 1977 Waves on water jets. *J. Fluid Mech.* **83**, 119–127.

Krulle, G., Mayer, W. & Schley, S. 1990 Recent advance in $H_2/O_2$ high pressure coaxial injector performance analysis. *AIAA Paper* 90-1959.

Lefebvre, A. H. 1989 *Atomization and Sprays*. Hemisphere.

Levich, V. G. 1962 *Physicochemical Hydrodynamics*. Prentice-Hall.

Li, X. 1995 Mechanism of atomization of a liquid jet. *Atomization Sprays* **5**, 89–105.

Li, X. & Shen, J. 1998 Absolute and convective instability of cylindrical liquid jets in co-flowing gas streams. *Atomization Sprays* **8**, 45–62.

Lian, Z. W. & Lin, S. P. 1990 Breakup of a liquid jet in a swirling gas. *Phys. Fluids* A **2**, 2134–2139.

Liao, Y. 1999 Instability and breakup of liquid sheets and liquid jets. PhD thesis, University of Cincinnati, Ohio.

Liao, Y., Jeng, S. M., Jog, M. A. & Benjamin, M. A. 1998 Atomization of a liquid jet under swirling air stream. *SAE Paper* 982612.

Liao, Y., Jeng, S. M., Jog, M. A. & Benjamin, M. A. 1999*a* Instability of an annular liquid sheet surrounded by swirling airstreams. *AIAA J.* **38**, 453–460.

Liao, Y., Sakman, A. T., Jeng, S. M., Jog, M. A. & Benjamin, M. A. 1999*b* A comprehensive model to predict simplex atomizer performance. *Trans. ASME: J. Engng Gas Turbines Power* **121**, 285–294.

Lin, S. P. & Chen, J. N. 1998 Role played by the interfacial shear in the instability mechanism of a viscous liquid jet surrounded by a viscous gas in a pipe. *J. Fluid Mech.* **376**, 37–51.

Lin, S. P. & Ibrahim, E. A. 1990 Instability of a viscous liquid jet surrounded by a viscous gas in a vertical pipe. *J. Fluid Mech.* **218**, 641–658.

Lin, S. P. & Kang, D. J. 1987 Atomization of a liquid jet. *Phys. Fluids* A **30**, 2000–2006.

Lin, S. P. & Lian, Z. W. 1990 Mechanism of the breakup of liquid jets. *AIAA J.* **28**, 120–132.

Lin, S. P. & Reitz, R. D. 1998 Drop and spray formation from a liquid jet. *Ann. Rev. Fluid Mech.* **30**, 85–105.

Lin, S. P. & Webb, R. 1994 Nonaxisymmetric evanescent waves in a viscous liquid jet. *Phys. Fluids* A **6**, 2545–2547.

Mansour, A. & Chigier, N. 1994 Effect of turbulence on the stability of liquid jets and resulting droplet size distributions. *Atomization Sprays* **4**, 583–604.

Ramamurthi, K. & Madhavan, N. G. 1998 Coaxial swirl injector element for a tripropellent engine. *AIAA Paper* 98-3514.

Ranz, W. E. 1958 Some experiments on orifice sprays. *Can. J. Chem. Engng* **36**, 175–181.

Rayleigh, Lord 1892 On the instability of a cylinder of viscous liquid under capillary force. *Phil. Mag*. **34**, 145–154.

Reitz, R. D. 1987 Modeling atomization processes in high-pressure vaporizing sprays. *Atomization Spray Technol*. **3**, 309–337.

Reitz, R. D. & Bracco, F. V. 1982 Mechanism of atomization of a liquid jet. *Phys. Fluids* **25**, 1730–1742.

Reitz, R. D. & Bracco, F. V. 1986 Mechanism of breakup of round liquid jets. In *Encyclopedia of Fluid Mechanics*, vol. 3 (ed. N. Cheremisinoff), pp. 233–249. Gulf.

Sterling, A. H. & Sleicher, C. A. 1975 The instability of capillary jets. *J. Fluid Mech*. **68**, 477–495.

Weaving, J. H. 1990 *Internal Combustion Engineering Science and Technology*. Elsevier.

Yang, H. Q. 1992 Asymmetric instability of a liquid jet. *Phys. Fluids* A **4**, 681–689.